ELSEVIER

1 May 1996

OPTICS COMMUNICATIONS

Optics Communications 126 (1996) 175–184

Full length article

Intensity-dependent absorption and its modelling in infrared sensitive rhodium-doped $BaTiO_3$

M. Kaczmarek [a,1], G.W. Ross [a], R.W. Eason [a], M.J. Damzen [b], R. Ramos-Garcia [b,2], M.H. Garrett [c]

[a] *Optoelectronics Research Centre and Department of Physics, University of Southampton, Southampton, SO17 1BJ, UK*
[b] *The Blackett Laboratory, Imperial College, Prince Consort Rd., London SW7 2BZ, UK*
[c] *Deltronic Crystal Industries Inc., 60 Harding Avenue, Dover, NJ 07801-4710, USA*

Received 20 October 1995; accepted 19 December 1995

Abstract

We investigate the intensity-dependent absorption coefficient of photorefractive Rh:$BaTiO_3$ from the maximum (633 nm) to the near infra-red end (1.06 μm) of this crystal's sensitivity. A numerical photorefractive model, incorporating dual-wavelength illumination and a secondary photorefractive centre, gives good agreement with experiment and shows that such a two-centre model is sufficient to explain the results obtained in the visible and infrared wavelength region.

1. Introduction

The photorefractive crystal $BaTiO_3$ has been the subject of many experimental and theoretical investigations due to its attractive nonlinear optical properties, which permit high two-beam coupling gain and large self-pumped phase conjugate reflectivities, without the need for an externally applied electric field. Past research has focused principally on the visible wavelengths where crystal response has been most efficient in undoped samples. Recently interest has turned towards near-infrared wavelengths, compatible with diode-pumped solid state lasers and semiconductor lasers, with applications such as diode injection locking [1] and brightness enhancement [2].

A new type of $BaTiO_3$, blue in colour, possesses enhanced absorption in the red and near infrared regions of the spectrum [3]. Fig. 1 shows the absorption spectrum of such a sample together with a nominally undoped sample of $BaTiO_3$ for comparison. Attempts to identify the impurity centre responsible for the blue colour and enhanced photorefractive response in the infrared region have suggested that rhodium (in the valence states Rh^{3+}/Rh^{4+}) may be responsible [4,5]. Through systematic addition of rhodium to the crystal melt, Wechsler and his colleagues obtained crystals which shared not only a remarkably similar absorption profile to that shown

[1] On leave from Department of Physics, A. Mickiewicz University, 60-780 Poznań, Poland.

[2] On leave from Instituto Nacional de Astrofísica, Optica y Electronica, Apdo. Postal 51 y 216, 72000 Puebla, Pue. Mexico.

PII S0030-4018(96)00046-6

in Fig. 1, but also similar optical and photorefractive characteristics to those reported in Ref. [3], [6]. The blue colour of Rh:$BaTiO_3$ is the result of higher absorption in the red than in the blue or green spectral region (Fig. 1). Additional analysis of a similar crystal by spark source mass spectroscopy, rhodium doping experiments [7] and electron paramagnetic resonance [8] showed that both Rh and Fe were present, and that the regions of higher absorption can be associated with the charge-transfer transitions involving the valence band edge and Rh^{4+} states which lie in the band gap [7].

In a recent paper, Kröse and coworkers [9] identified energy levels of as-grown $BaTiO_3$ containing rhodium by performing simultaneous measurements of light-induced electron spin resonance and optical absorption. They found that depending on the energy of light, holes can be transferred between Rh^{4+} and Fe^{3+} ($1.2\ eV < E < 2.5\ eV$) or from Fe^{4+} to Rh^{3+} and to an unknown hole trap ($E > 2.5$ eV).

Our earlier studies [10] showed that light-induced transparency can be observed in Rh:$BaTiO_3$, and we have already successfully modelled the experimental data using a two-centre model. In this paper, we present our further experimental and theoretical investigations of single and dual-wavelength intensity-dependent absorption measurements in this infrared sensitive blue Rh:$BaTiO_3$ crystal over a wide range of wavelengths. We use a two-centre (deep and shallow trap) model modified to incorporate simultaneous illumination by two different wavelengths, which has enabled us to characterise the effective values of parameters of the second centre including the wavelength dependence of the photoionisation cross-section.

2. Theory

It has already been shown that intensity-dependent absorption is consistent with the presence of secondary centres [11,12]. These are intermediate-level charge trapping impurity sites that are usually highly ionised at room temperature, but can be populated by photoionised charge carriers from the deep centres. The photoinduced transfer of charge from a deep to a secondary centre leads to a change in the absorption of the crystal if different photoionisation cross-sections exist for these centres. Direct intra band charge transfer is also, in principle possible, but it is not usually included in band-transport models.

Typical photoinduced absorption measurements [13] involve the transmission of a weak incoherent beam through a photorefractive crystal to monitor

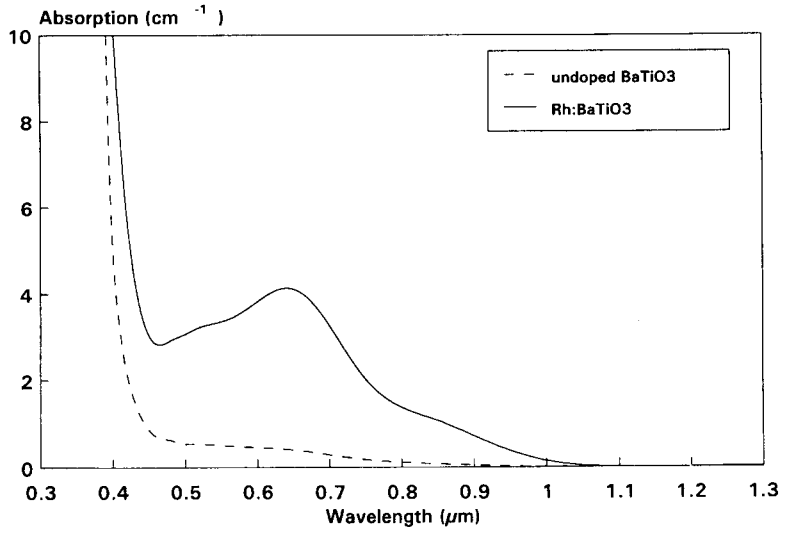

Fig. 1. Absorption spectrum of infrared-sensitive Rh:$BaTiO_3$ using light polarised parallel to the crystal c-axis is shown as the solid line. For comparison the spectrum of typical as-grown $BaTiO_3$ crystal is shown as the dashed line.

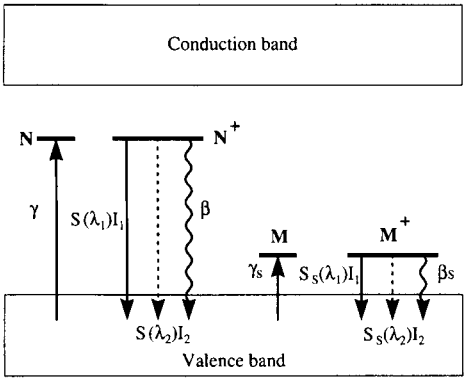

Fig. 2. Model energy diagram of photorefractive infrared-sensitive $BaTiO_3$ with deep and secondary (shallow) centres and two wavelength illumination.

the changes in the absorption induced by varying a strong pump beam. In our experiments we have varied the intensity of both beams, which are at different wavelengths, and then extended the two-centre photorefractive model to include this feature. The advantage of using the dual wavelength illumination technique is that it enables us to deduce the effective magnitudes of a wider range of parameters than the ones obtained using a single-wavelength illumination.

A model that incorporates the secondary centres and dual-wavelength illumination is shown schematically in Fig. 2, where we have assumed a hole-dominated crystal in accordance with other rhodium doped crystals [6]. In our notation N and N^+ are the densities of the deep centres with total deep centre density $N_D = N + N^+$, M and M^+ are the densities of shallow centres with total shallow centre density $M_T = M + M^+$. The parameters S, β, and γ are, respectively, the cross-section for photoionisation, rate of thermal ionisation and coefficient of recombination. The unsubscripted parameters refer to the deep centres and the corresponding parameters with subscript "s" refer to secondary-trap coefficients. I_1 and I_2 are the intensities of beams 1 and 2 with wavelengths λ_1 and λ_2, respectively.

In our analysis we start with the material equations for the two-centre model presented previously [11,12]. To introduce the two wavelength illumination we note that beams 1 and 2 are necessarily mutually incoherent so no beam coupling is observed, and the presence of the second beam (λ_2) can be simply represented by an intensity dependent contribution to the thermal ionisation rates of the deep and secondary centres and given by

$$\beta(I_2) = \beta + S(\lambda_2) I_2, \tag{1}$$

$$\beta_s(I_2) = \beta_s + S_s(\lambda_2) I_2, \tag{2}$$

where $S(\lambda_2)I_2$ and $S_s(\lambda_2)I_2$ are the photoionisation rates due to beam 2. In order to calculate the intensity dependence of the absorption coefficient, we have assumed uniform illumination for both beams, and solved the material equations in steady-state. The absorption coefficient observed at wavelength λ_1 due to the presence of both beams is given then by the equation [10]:

$$M^+ = \frac{1}{2\rho(I_1, I_2) - 1} \times \Big\{ \big[\rho(I_1, I_2)(N_D + M_T) + N_D - N_A \big] - \big[(\rho(I_1, I_2)(N_D + M_T) + N_D - N_A)^2 - 4\rho(I_1, I_2)(\rho(I_1, I_2) - 1) N_D M_T \big]^{1/2} \Big\} \tag{3}$$

and

$$\rho(I_1, I_2) = \frac{\gamma_s S(\lambda_1)}{\gamma S_s(\lambda_1)} \left(\frac{1 + \beta(I_2)/S(\lambda_1) I_1}{1 + \beta_s(I_2)/S_s(\lambda_1) I_1} \right), \tag{4}$$

$\alpha(0) = (hc/\lambda) S N_A$ is the low intensity absorption coefficient when $I_1 \approx I_2 \approx 0$, N_A is the concentration of compensating acceptors, and $M^+(I_1, I_2)$ is the population of shallow traps filled with holes due to photoinduced transfer of charge from the deep to the shallow levels and is a saturating function of intensity [12]. Analysis shows that strong intensity-induced filling of the secondary centres occurs at a characteristic saturation intensity given by $I_{sat} = \beta_s/S_s$ when illuminated with a single beam [11,14,15]. It is noted that due to the wavelength dependence of S_s, I_{sat} is also wavelength dependent. In the case of dual wavelength illumination the rate of thermal ionisation β_s, at one wavelength can also

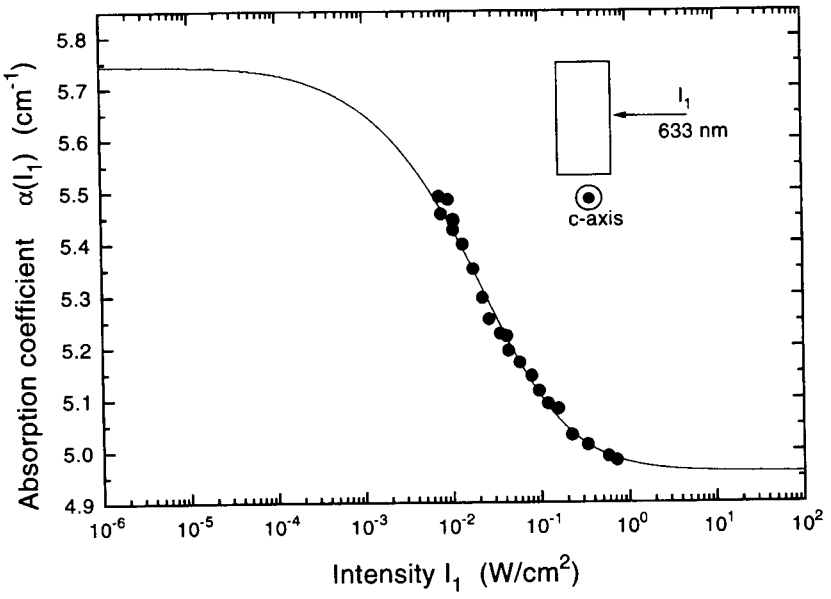

Fig. 3. Intensity-dependence of the absorption coefficient at 633 nm showing light-induced transparency. The full dots are experimental data and solid curve is theoretical simulation based on the parameters of Table 1.

be made effectively intensity dependent due to the presence of the other beam according to Eq. (2).

3. Experimental results

In the first experiment we aimed at investigating the photoinduced absorption change at the peak of the absorption spectrum of Rh:$BaTiO_3$, i.e. around 640 nm. The transmission of an o-polarised He-Ne beam propagating through the Rh:$BaTiO_3$ crystal sample with dimensions $7.3 \times 5.6 \times 3.0$ mm^3 (see inset of Fig. 3) was measured. The use of the o-polarised light minimises self-induced holographic scattering. Fig. 3 shows a plot of the absorption coefficient as a function of the incident intensity of the He-Ne beam. The graph indicates an intensity dependent reduction of the absorption coefficient corresponding to light-induced transparency with $S_s(\lambda_1) < S(\lambda_1)$ [16]. This is the reverse effect compared to observations in as-grown $BaTiO_3$ samples [12], where intensity-dependent induced absorption

Table 1
Crystal parameters used in numerical simulations

	Deep centres	Secondary centres
Density of species	$N_D = N + N^+ = 2.02 \times 10^{18}$ cm^{-3}	$M_T = M + M^+ = 1.1 \times 10^{18}$ cm^{-3}
	$N_{dark} = N_D - N_A = 2 \times 10^{16}$ cm^{-3}	$M^+_{dark} = 0$
Photoexcitation cross section at 514 nm	$S = 5.0$ cm^{2}J^{-1}	$S_s = 1.8$ cm^{2}J^{-1}
Photoexcitation cross section at 633 nm	$S = 9$ cm^{2}J^{-1}	$S_s = 1.6$ cm^{2}J^{-1}
Photoexcitation cross section at 647 nm	$S = 9.2$ cm^{2}J^{-1}	$S_s = 1.8$ cm^{2}J^{-1}
Photoexcitation cross section at 750 nm	$S = 4.1$ cm^{2}J^{-1}	$S_s = 2.0$ cm^{2}J^{-1}
Photoexcitation cross section at 800 nm	$S = 3.8$ cm^{2}J^{-1}	$S_s = 2.1$ cm^{2}J^{-1}
Photoexcitation cross section at 1.06 μm	$S = 0.02$ cm^{2}J^{-1}	$S_s = 0.25$ cm^{2}J^{-1}
Thermal excitation rate	$\beta = 5 \times 10^{-4}$ s^{-1}	$\beta_s = 0.1$ s^{-1}
Recombination coefficient ratio γ_s/γ	0.5	0.5

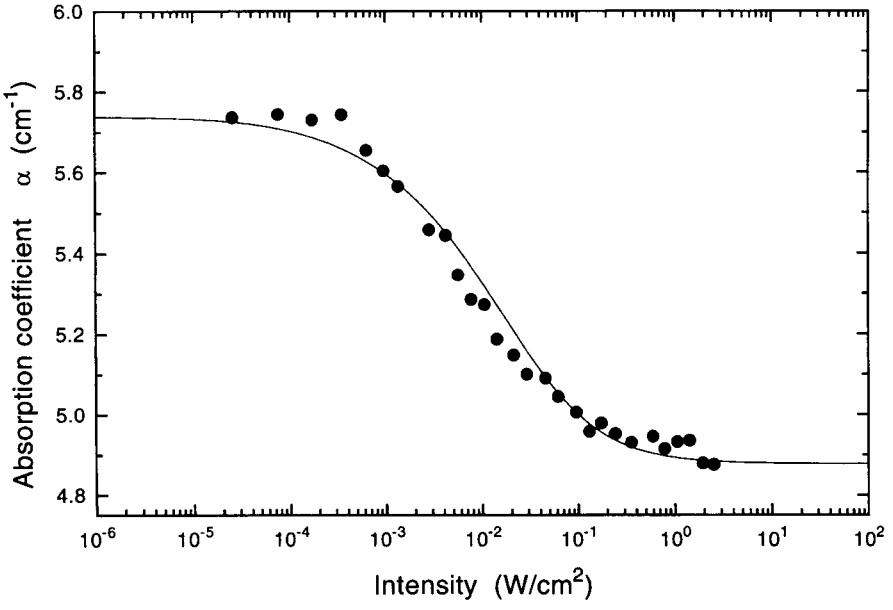

Fig. 4. Intensity-dependence of the absorption coefficient at 647 nm showing light-induced transparency. The full dots are experimental data and solid curve is theoretical simulation based on the parameters of Table 1.

has been observed ($S_s(\lambda_1) > S(\lambda_1)$). The solid line shown in Fig. 3 (and in other figures) is a theoretical curve obtained from the numerical simulations of our model described in the previous section and using the parameters listed in Table 1.

To test the consistency of the agreement between

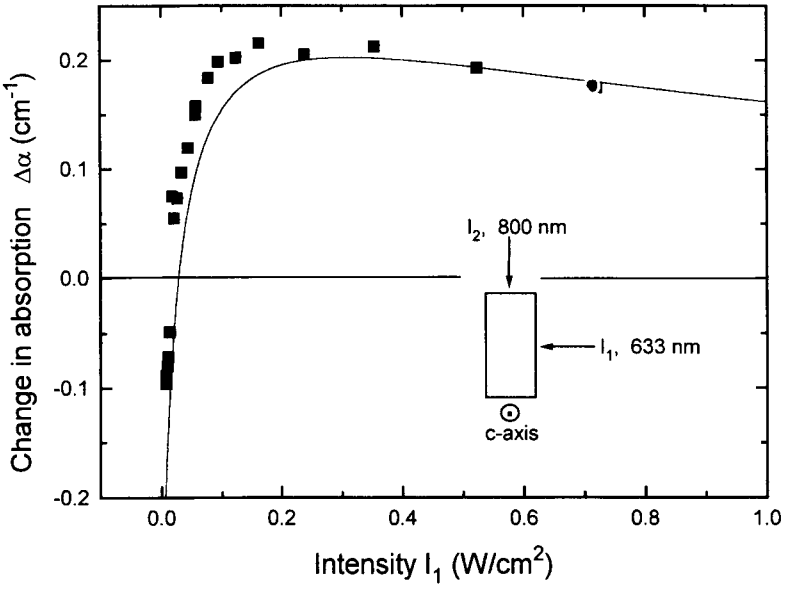

Fig. 5. Change in the absorption coefficient at 633 nm as a function of the He-Ne intensity I_1 with and without secondary illumination beam I_2(800 nm) = 1.3 W/cm^2. Full dots are experimental data taken as shown in inset, solid line is a theoretical curve based on the parameters given in Table 1.

theory and experiment we also performed intensity-dependent absorption measurements at a wavelength of 647 nm as shown in Fig. 4, over a range of intensities exceeding five decades. We observed the decrease in the absorption coefficient by as much as 0.9 cm^{-1}. The wavelength 647 nm corresponds approximately to the peak of the absorption spectra. With a common set of parameters, the theoretical model was able to reproduce experimental data very well. It is worth noting that the saturation intensity at 647 nm is smaller than the saturation intensity at 633 nm due to the larger cross-section of the shallow traps at 647 nm.

The measurements of intensity-dependent change in the absorption coefficient were also performed at 800 nm. Investigations of the effect of single-wavelength illumination of $Rh:BaTiO_3$ with 800 nm originating from a Ti:sapphire laser showed that no significant, reliable, measurable changes in absorption could be detected. This would be consistent with $S_s \approx S$ in this wavelength region. It may be interesting to recall here the dual-wavelength (633 and 800 nm) results obtained earlier [9]. In that experiment, the $Rh:BaTiO_3$ crystal was illuminated by two o-polarised beams, a He-Ne beam at $\lambda_1 = 633$ nm, and a near infrared beam at $\lambda_2 = 800$ nm from a Ti:sapphire laser. The arrangement of the beams was as shown in the inset of Fig. 5. The He-Ne beam intensity, I_1, was varied and then its transmission measured with and without the infrared beam at 800 nm, whose intensity was kept at 1.3 W/cm^2. The change in absorption coefficient, according to Eq. (3), with and without the secondary beam I_2, can be written as $\Delta\alpha(I_1) = \alpha(I_1, I_2 = 1.3\ W/cm^2) - \alpha(I_1, 0)$. A graph showing $\Delta\alpha$ as a function of the He-Ne intensity I_1 is illustrated in Fig. 5. The results obtained can be explained as follows. At low intensities of the 633 nm beam, and without the 800 nm beam present, the absorption coefficient would be approximately equal to $\alpha(0)$, namely $\alpha(I_1, 0) = \alpha(0)$. The presence of the 800 nm beam changes this condition and a low intensity He-Ne beam experiences the absorption coefficient $\alpha(I_1, I_2)$ which is smaller than $\alpha(0)$. This is the result of the intensity of the near-infrared beam I_2 being high enough to induce charge transfer of carriers from the deep traps to the shallow traps. Thus, at low intensity the He-Ne beam will see a more transparent crystal with I_2 than without it, corresponding to a negative value of $\Delta\alpha$.

Another consequence of the presence of the near-

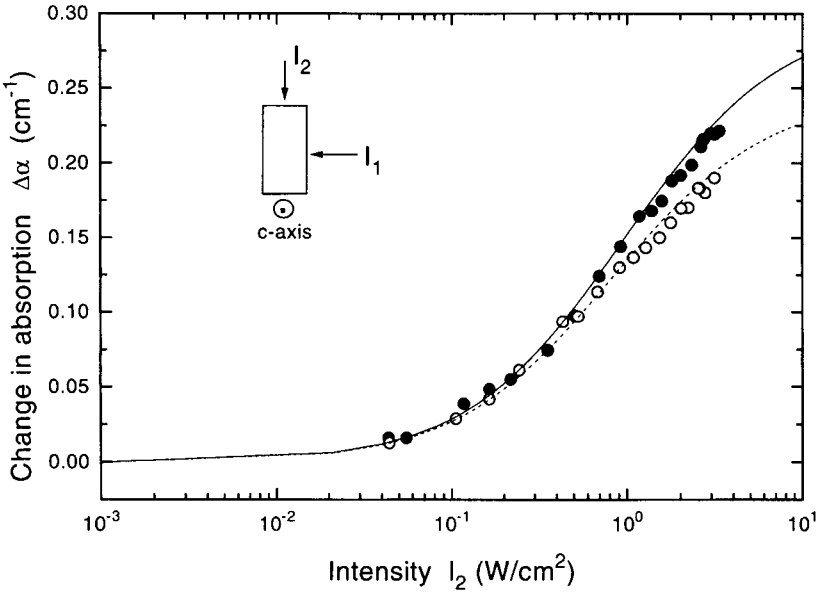

Fig. 6. Change in the absorption coefficient at 633 nm with fixed intensity I_1 as a function of the secondary illumination beam with intensity I_2 at two different wavelengths. Full dots ($\lambda_2 = 800$ nm) and open dots ($\lambda_2 = 750$ nm) are experimental data. Solid line ($\lambda_2 = 800$ nm) and dashed line ($\lambda_2 = 750$ nm) are theoretical curves based on the parameters given in Table 1.

infrared beam is to change the effective thermal rate $\beta_s(I_2)$ seen by beam I_1, and this causes a shift in the saturation intensity $I_{sat} = \beta_s(I_2)/S_s(\lambda_1)$ to higher values, making the shallow traps harder to saturate. If we further increase the He-Ne intensity, the change in the absorption diminishes and eventually changes sign as shown in Fig. 5. We have also shown theoretically that there is a certain value of intensity I_1, at which, regardless of the intensity of the beam I_2, no change in the absorption coefficient is induced, and that this particular intensity of I_1 is a function of the crystal's parameters [9].

In the second experiment we arranged the He-Ne laser beam to have a fixed intensity $I_1 = 0.85$ W/cm^2. This intensity I_1 corresponds to a strongly saturated condition of the induced transparency according to Fig. 3. The change in transmission of the He-Ne beam was then monitored as a function of the intensity of the infrared beam, I_2. The graphs in Fig. 6 show the change in the absorption coefficient as a function of the near-infrared illumination I_2 for the two cases of $\lambda_2 = 800$ nm and 750 nm. According to Eq. (3), the dual-wavelength change in absorption coefficient in this case can be written as $\Delta\alpha(I_2) = \alpha(I_1 = 0.85\ \text{W/cm}^2, I_2) - \alpha(I_1 = 0.85\ \text{W/cm}^2, 0)$. The solid and dashed curves show the theoretical modelling for $\lambda = 800$ nm and $\lambda = 750$ nm, respectively. Because of the increase of the effective thermal rate, according to Eq. (2), we expect an increase in the depopulation rate of the shallow traps. The infrared beams have the effect of sending the charge back from the shallow to deep traps, increasing their population. The result of this process is, again, a smaller magnitude of light-induced transparency. In other words, fast transfer of holes back into the deep traps will result in an overall reduction of $M^+(I_1,I_2)$, and therefore the He-Ne experiences a reduction of the induced transparency according to Eq. (3).

Finally, Fig. 7 shows the results of intensity-dependent *absorption* at 1.06 μm. There are two important, characteristic features which can be observed. First, our measurements show induced absorption, corresponding to $S_s(\lambda_1) > S(\lambda_1)$, i.e. the opposite to what we obtained in the red region of the spectrum. Secondly, the saturation intensity is approximately an order of magnitude bigger than the one at visible illumination, as a result of the smaller photoionisation cross-section of the shallow traps. In addition, this magnitude of the photoionisation cross-section results in small induced absorption,

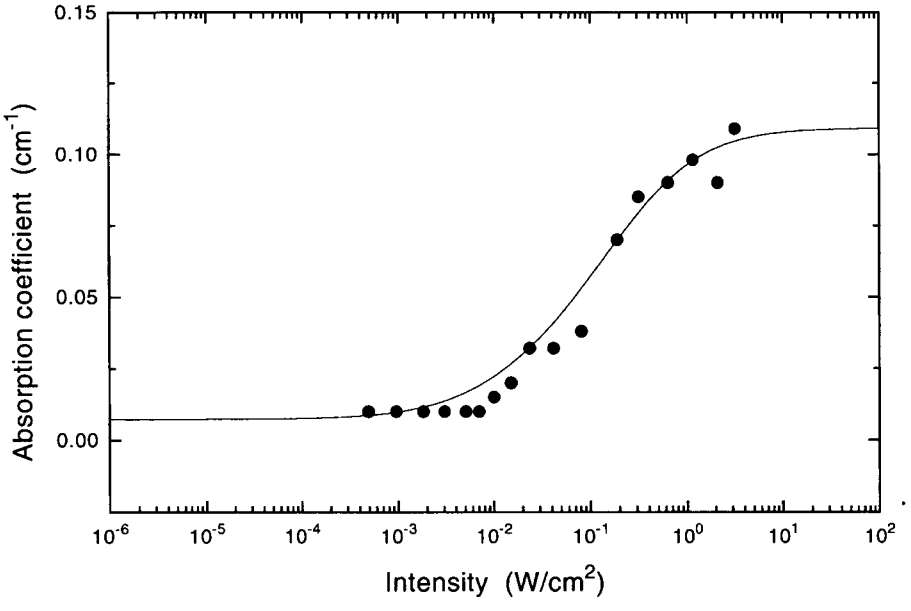

Fig. 7. Intensity-dependence of the absorption coefficient at 1.06 μm showing light-induced absorption. The full dots are experimental data and solid curve is theoretical simulation based on the parameters of Table 1.

given by Eq. (3). Note that the low intensity absorption coefficient at 1.06 μm (due to the deep centres) is quite low (≤ 0.03 cm^{-1}) and this is the reason why the condition $S_s(\lambda_1) > S(\lambda_1)$ can be fulfilled at this wavelength.

4. Discussion of results and model parameters

A summary of the crystal parameters used in our numerical simulations is shown in Table 1, and their values were deduced mostly from our measurements. By measuring the two-beam coupling gain coefficient at 647 nm and intensity $I = 0.27$ W/cm^2 as a function of the grating wavevector, we estimated the effective trap density to be N_{eff} (where we assume that $N_{eff} \sim N \sim N_D - N_A) = 2 \times 10^{16}$ cm^{-3} [17]. This effective trap density is determined via the Debye screening wavevector. However, in the presence of both deep and shallow traps, the Debye screening wavevector becomes intensity-dependent, and the straightforward relation which takes its magnitude as the value of the grating wavevector at which the space-charge field is maximum [18] is strictly not valid anymore. But although the intensity at which the effective trap density was determined in our case was high enough to induce some filling of the shallow traps, theoretical calculations show that a shift of only $\sim 20\%$ is expected in the magnitude of the optimum grating wavevector as compared to its value at low intensity. We therefore consider our measured value to be a reasonable estimate for N_{eff}.

The wavelength-dependent absorption coefficient at low intensity $\alpha_0(\lambda) \approx (hc/\lambda)S(\lambda)N^+$, assumed to be due to hole photoionisation from the dark value of the positively-charged deep centre species ($N^+ = N_A$), can be used to determine the photoionisation cross-section of deep traps. At this point, we need to make some assumptions because neither N_A nor N_D are known separately and further experiments must be done to find their values. In hole-dominated crystals, like ours, the ratio between donors and ionised donors $r = N/N^+$ should be quite small, a typical value for this ratio in as-grown samples of $BaTiO_3$ is around $r \sim 0.01$ [17], which we take for our modelling. From the intensity-dependent absorption data shown in Fig. 3, we determine the characteristic saturation intensity for shallow trap filling as $I_{sat} = \beta_s/S_s \sim 22$ mW/cm^2 at $\lambda_1 = 633$ nm. Dark decay measurements of the observed changes in the absorption were characterised by a dominant slow recovery (a few seconds). The time scales of the process was intensity-dependent: occurring faster for higher intensities, in agreement with previous observations [13]. From the measured time of dark decay recovery of induced absorption, ~ 6–10 s, we estimate $\beta_s \sim 0.1$ s^{-1} With these parameters we found fitted values for the shallow trap photoionisation cross-section $S_s \sim 9$ cm^2 J^{-1} at $\lambda = 633$ nm and total density of shallow traps $M_T \sim 1.1 \times 10^{18}$ cm^{-3} from intensity-dependent induced transparency measurements.

In order to verify the consistency of our model with these parameters, we modelled the dark decay measurements of the induced absorption by solving numerically the material equations at zero order, i.e. at negligibly small values of incident light intensity. Our model predicted a dark decay time of ~ 10 s, in agreement with the experiment. Additionally, the modelling of dark decay allows us to estimate the magnitude of the shallow trap to deep trap recombination rates, γ_s/γ, since the temporal behaviour of dark decay of the change in absorption coefficient (αM^+) is given by the following equation

$$\frac{\partial M^+}{\partial t} = -\frac{\beta_s M^+}{1 + \gamma_s M/\gamma N}, \tag{5}$$

where $M = M_T - M^+(t)$ and $N = N_D - N_A + M^+(t)$ are time dependent and the decay will be nonexponential in form. The ratio $\gamma_s M/\gamma N$ is physically equal to the average number of times the thermally-ionised carrier from a filled shallow level is retrapped back into the shallow trap before it recombines with a deep trap. From Eq. (5), it can be seen that the exponential decay time (τ_D) measured experimentally is an approximation to the reciprocal of a weighted time-average decay rate and therefore within the limits $\beta_s/(1 + \gamma_s M_T/\gamma(N_D - N_A)) < \tau_D^{-1} < \beta_s$. By trial and error we look for the values that simultaneously fit best both the intensity-dependent absorption coefficient and the dark decay of induced transparency, to obtain a value for $\gamma_s/\gamma = 0.5$.

Once we have characterised the shallow traps at a

given wavelength we can easily find the values of the photoionisation cross-section of the traps at any second wavelength with the help of the low intensity absorption spectrum and by fitting the change in the absorption coefficient $\Delta\alpha$ to experimental data. The deep trap cross section $S(\lambda_1)$ at any other wavelength λ_1 can be found, if we know its low intensity absorption coefficient $\alpha(\lambda_1)$, from $S(\lambda_1) = [\lambda_0\alpha(\lambda_0)/\lambda_0\alpha(\lambda_1)]S(\lambda_0)$ where $S(\lambda_0)$ and $\alpha(\lambda_0)$ are the cross-section, wavelength and low-intensity absorption of the already characterised deep trap at the wavelength λ_0. This method reproduces particularly well the experimental results from the red and infrared wavelengths region.

The extended range of wavelengths we have considered allowed us to estimate better than before [9] the magnitude of the deep and shallow traps parameters. However, we call these parameters *effective*, as they are not determined uniquely. It is nevertheless possible to draw some general conclusions and interesting observations, characterising the behaviour of our Rh:$BaTiO_3$ crystals. The most important fact is that the change of absorption we observed at wavelengths from 514.5 nm to 1.06 μm could all be simulated using the two-level model.

We observed that the condition $S_s(\lambda_1) < S(\lambda_1)$ is fulfilled in the red region of the spectrum, and as a result induced transparency is observed. When we moved towards longer wavelengths, the cross-section of the deep trap decreases, following the absorption coefficient spectrum (Fig. 1), until eventually the previous condition reverses becoming $S_s(\lambda_1) > S(\lambda_1)$, corresponding to the effect of induced absorption as seen at 1.06 μm. There is a crossover point when $S_s(\lambda_1) = S(\lambda_1)$ somewhere between the wavelength region of 800 nm and 1 μm. A similar wavelength dependent absorption/transparency behaviour has been observed in a reduced sample of Rh:$BaTiO_3$, but no systematic intensity-dependent absorption measurements were presented [16]. Our theoretical results show that the cross-section of the shallow traps remains constant over a wide range of wavelengths as shown in Table 1. Attempts to extend our model to shorter wavelengths, for example in the blue-green region of the spectrum [9], gives only qualitative agreement with the experiment. We speculate that other effects, not included in this model, such as electron–hole [18] competition and multiple shallow trap levels [19] may cause deviations of the experimental results from the present model.

Recent work on other Rh:$BaTiO_3$ crystals has shown that in the green-blue region of the spectrum at least three photorefractive centres are necessary to explain the data [7]. We found no experimental evidence to substantiate such a model in our case.

5. Conclusions

In summary, we have presented results of single and dual wavelength intensity-dependent absorption measurements over a wide range of the spectrum (633 nm–1.06 μm) in an infrared sensitive Rh:$BaTiO_3$ crystal. We have observed induced transparency at red and near infrared (633–800 nm) illumination and induced absorption at 1.06 μm illumination. The results of single-wavelength and dual-wavelength intensity dependent absorption coefficients have been modelled numerically and from the numerical fit we were able to identify the effective values of deep and secondary centre parameters. Moreover, we showed that in our dual wavelength illumination scheme, the presence of one of the beams allows one to control the amount of induced absorption/transparency that is experienced by the other beam. The good agreement between experiment and theory, which uses a common set of parameters to model all cases, indicates that the two-centre model can explain the intensity dependent behaviour of this new doping of Rh:$BaTiO_3$ crystal in the red and near-infrared regions of the spectrum.

Acknowledgements

We would like to thank Petr Hribek from the Technical University in Prague for his help in experimental studies of Rh:$BaTiO_3$ and Daniel Rytz of Forschungsinstitut für mineralische und metallische Werkstoffe, Edelsteine/Edelmetalle GmbH in Idar-Oberstein in Germany for his collaboration in the work on Rh:$BaTiO_3$. We also thank Dr. Dave Richardson for the loan of his YAG laser, and the Laser Division, Rutherford Appleton Laboratory, Chilton, Didcot, UK, for the Ti:sapphire used in this

research. RRG would like to acknowledge the financial support from CONACyT, Mexico.

References

[1] S. MacCormack, J. Feinberg and M.H. Garrett, CLEO Technical Digest 11 (1993) CThS55.
[2] S. MacCormack and J. Feinberg, CLEO Technical Digest 11 (1993) CTuN19.
[3] G.W. Ross, P. Hribek, R.W. Eason, M.H. Garret and D. Rytz, Optics Comm. 101 (1993) 60.
[4] C. Warde, T.S. McNamara. M.H. Garrett and P. Tayebati, SPIE Conference, San Diego, CA (1993) CR48-07.
[5] T.W. McNamara, S.G. Conahan, I. Mnushkina, M.H. Garret, H.P. Jensen, C. Warde, SPIE Critical Review Proceedings, Vol. CR-48, eds. P. Yeh and C. Gu (1994).
[6] B.A. Wechsler, M.B. Klein, C.C. Nelson and R.N. Schwartz, Optics Lett. 19 (1994) 536.
[7] M.H. Garrett, H.P. Jensen, C. Warde, G.D. Bacher, S. MacCormack, J. Feinberg and R.N. Schwartz, private communication.
[8] EPR measurements made by R.N. Schwartz, Hughes Research Lab, Malibu, CA.
[9] H. Kröse, E. Possenriede, R. Scharfschwerdt, T. Varnhorst, O.F. Schirmer, H. Hesse and C. Kuper, Opt. Mater. 4 (1995) 153.
[10] M. Kaczmarek, G.W. Ross, P.M. Jeffrey, R.W. Eason, P. Hribek, M.J. Damzen, R. Ramos-Garcia, R. Troth, M.H. Garrett and D. Rytz, Opt. Mater. 4 (1995) 158.
[11] G.A. Brost, R.A. Motes and J.R. Rotgé, J. Opt. Soc. Am. B 5 (1988) 1879.
[12] P. Tayebati and D. Mahgerefteh, J. Opt. Soc. Am. B 8 (1991) 1053.
[13] G.A. Brost and R.A. Motes, Optics Lett. 15 (1990) 538.
[14] R.A. Motes, G.A. Brost, J.R. Rotgé and J.J. Kim, Optics Lett. 13 (1988) 509.
[15] D. Mahgerefteh and J. Feinberg, Phys. Rev. Lett. 64 (1990) 2195.
[16] M.H. Garrett, P. Tayebati, J.Y. Chang, H.P. Jenssen and C. Warde, J. Appl. Phys. 72 (1992) 1965.
[17] M. Kaczmarek, P. Hribek and R.W. Eason, Characterisation of photorefractive properties of "blue" Rh:BaTiO3 via nonlinear wave mixing, J. Modern Optics, to be published.
[18] M.B. Klein, in: Photorefractive Materials and Their Applications, eds. I.P. Günter and J.-P. Huignard (Springer, Heidelberg, 1987) Chap. 7, p. 229.
[19] R.S. Cudney, R.M. Pierce, G.D. Bacher and J. Feinberg, J. Opt. Soc. Am. B 8 (1991) 1326.